JOURNAL OF CATALYSIS 124, 268–280 (1990)

Designing Zeolite Catalysts for Shape-Selective Reactions: Chemical Modification of Surfaces for Improved Selectivity to Dimethylamine in Synthesis from Methanol and Ammonia

DAVID R. CORBIN,[1] MICHAEL KEANE, JR., LLOYD ABRAMS, RODNEY D. FARLEE, PAUL E. BIERSTEDT, AND THOMAS BEIN[2]

Central Research and Development Department,[3] E. I. du Pont de Nemours and Company, Inc., Experimental Station, P.O. Box 80262, Wilmington, Delaware 19880-0262

Received December 20, 1989; revised February 21, 1990

The relative contributions of external and intracrystalline acidic sites of small pore H-*R*HO zeolite for the selective synthesis of methylamines from methanol and ammonia have been studied. Nonselective surface reactions which produce predominantly trimethylamine can be eliminated by "capping" the external acidic sites with trimethylphosphite (TMP) and other reagents, thus improving the selectivity toward the formation of dimethylamine. For small pore zeolites, neither the zeolite pore size nor the internal acidic sites is significantly affected by this treatment. *In situ* infrared and MAS-NMR studies show that TMP reacts irreversibly with the zeolite acidic sites via a modified Arbusov rearrangement to form surface-bound dimethylmethylphosphonate.

INTRODUCTION

The industrial preparation of methylamines involves the reaction of methanol and ammonia over a solid-acid catalyst. The reaction proceeds toward a thermodynamic equilibrium distribution of the three amines which favors trimethylamine production. At 90% conversion of methanol, the equilibrium product distribution is 17 : 21 : 62 (mol%) of monomethylamine (MMA), dimethylamine (DMA), and trimethylamine (TMA), respectively. While TMA is favored, the greatest market demand is for DMA. Presently, unwanted TMA is reequilibrated with ammonia to produce MMA and DMA. This technique, though material efficient, is energy intensive. To improve the selectivity to DMA in this reaction, we have examined zeolites as potential catalysts (1–7).

Zeolites possess a variety of properties which make them attractive candidates as catalysts and/or supports for shape-selective reactions. These include molecular sieving ability, ion exchange capacity, and large, accessible surface area. Theoretically, the surface area of zeolites is on the order of 1200 m^2/g (vide infra). To put this into perspective, the surface area of zeolites has been described in terms of "a single cupful has enough surface area to cover 20 football fields" (*8*). As such almost every atom of the zeolite can act as a reactive site. Although a zeolite has a very large surface area, the external surface of the zeolite particles should account for only a very small percentage of the total surface area (dependent upon the particle size). Any catalytic sites on the external crystallite surface would be expected to be nonsize selective compared to those within the molecular sieving framework. Furthermore, one must also consider the accessible surfaces of any impurity phases that may be present. The contributions to the product distribution by the external, accessible surface must be

[1] To whom correspondence should be addressed.

[2] Present address: Department of Chemistry, University of New Mexico, Albuquerque, NM 87131.

[3] Contribution Number 5351.

0021-9517/90 $3.00

dealt with in order to take full advantage of the internal size selectivity of the zeolite.

Product distribution selectivity obtained using zeolites can generally be improved by decreasing the numbers of the unselective active sites by poisoning or blocking them by various treatments. For example, the external surface can be coated with a catalytically inactive molecule. This type of treatment could also lead to pore narrowing which can significantly affect the product distribution (*6, 7, 9*). Coke formation on the external surface, for example, has a significant effect on the shape selectivity exhibited by the zeolite in the conversion of methanol to hydrocarbons (*10*). Addition of a site-selective poison can also lead to improved selectivity (*11, 12*). For example, selective poisoning of metal sites on the external zeolite surface using bulky phosphines (*11*) or thiophene (*12*) was essential in order to obtain selectivity for olefin and acetylene hydrogenations, respectively. In this paper, we describe the vapor-phase treatment by trimethylphosphite and other reactive compounds of zeolites to improve their performance as catalysts in the selective synthesis of dimethylamine from methanol and ammonia.

EXPERIMENTAL

Zeolites. Zeolites *R*HO (*13*), ZK-5 (*14*), offretite (*15*), T (*16*), and ZSM-34 (*17*) were prepared by literature methods. A sample of chabazite (Durkee, OR) was obtained from Minerals Research. Samples of clinoptilolite (Zeolon 400, Lot No. SN 43281) and ferrierite (Zeolon 700, Lot No. 43118) were obtained from Norton Chemical. The ammonium forms of these zeolites were prepared by conventional ion exchange using 10% NH_4NO_3 solutions (10 ml/g) at 90°C for 1 h. This procedure was repeated twice. NH_4-Erionite (ELZ-E-6, Lot No. 44140-78) and ultrastable NH_4-Y (LZ-Y82, Lot No. 9661796179) were obtained from Linde. Acid forms were prepared by heating at 60°C/h to 550°C and then calcining at 550°C for 10 h.

"Vapor-phase" treatments were performed by contacting the dehydrated, hydrogen form of the zeolite with a vapor for a period of time (minutes to hours). Compounds used include trimethylphosphite (TMP), hexamethyldisilazane (HMDS), silicon tetrachloride ($SiCl_4$), chlorotrimethylsilane (Me_3SiCl), dichlorodimethylsilane (Me_2SiCl_2), triethylborate (TEB), titanylchloride ($TiOCl_2$), and phosphorus trichloride (PCl_3). An example of a preparation is given below.

Trimethylphosphite vapor-phase-treated H-RHO. Zeolite Na,Cs-*R*HO was contacted three times for about 1 h each with a 10% solution of NH_4NO_3 at 90°C, with filtering between each contact. The resulting material was then filtered, washed with distilled water, and dried. This product, NH_4–*R*HO, was calcined in air by raising the temperature 60°C per hour to a final temperature of 550°C and heating the material at 550°C for 10 h. With the exception of sample I (vide infra) with 2.8 Cs/unit cell, the samples of H-*R*HO examined contained between 0.25 and 0.97 Cs/unit cell.

Ten grams of this preparation of zeolite H-*R*HO was placed in a quartz tube in a vertically mounted tube furnace, heated by raising the temperature 60°C per hour to 550°C under flowing nitrogen, further heated at 550°C for 10 h under flowing nitrogen, and then cooled to room temperature. The dry sample, at 23°C, was then contacted with a stream of nitrogen that had first been passed through TMP. After 4 h of contact, the TMP supply was shut off, and the sample was left under flowing nitrogen for an additional 16 h. The resulting catalyst is labeled sample I. Using this procedure, H-*R*HO was treated with each of the compounds listed above. Conditions for additional, different treatments of other samples of H-*R*HO with TMP used for characterization studies are given in Table 1.

Treatment of other zeolites with TMP involved the following procedure. Five grams of each acid zeolite was placed in a quartz tube and heated, under flowing nitrogen, at

TABLE 1

TMP Treatment Conditions for H-*RHO*

Sample no.	Calcination temp. (°C)	Dehydration temp. (°C)	Treatment temp. (°C)	Post-treatment temp. (°C)
I	550	550	RT	RT
II	400	400	RT	RT
III	400	400	RT	200
IV	400	400	RT	350
V[a]	550	550	150	RT
VI	550	550	RT	RT
VII	550	700	150	RT
VIII	600	300	RT	200

[a] Used catalyst.

5°C/min in a vertical tube furnace to 300°C for 4 h and then cooled to room temperature. The dry sample was contacted with a stream of nitrogen that had been passed through TMP. After 4 h of contact, the TMP supply was shut off and the sample was heated at 200°C for 1 h under flowing nitrogen.

Reactor studies. Reactor operation was discussed in detail in Ref. (*3b*). Catalyst activity data are represented by space velocities obtained from the reactant feed rates and catalyst load. Space velocity data ("activity number") under identical reactor conditions (90% methanol conversion, 325°C, 1 : 1 NH_3-to-methanol feed composition, and 1 atm pressure) are used to provide a basis of comparison. Relative rate constants were calculated via methods described previously (*3b*).

Infrared. Infrared studies were performed with a Nicolet 3600 FTIR spectrometer. Sample pellets (approximately 10 mg) of 1.0 cm diameter were mounted in the spectrometer in an all-metal vacuum system having a base pressure of $<1 \times 10^{-8}$ Torr. The samples were contained, inside the vacuum system, in a quartz oven capable of heating the sample for dehydration purposes. Typically, the samples are dehydrated under vacuum at 450°C prior to analysis.

Solid-state NMR. Solid-state NMR experiments were performed with a Bruker CXP-300 spectrometer. For ^{31}P, a 30° to 90° pulse with 10 s recycle time was used, depending on the T_1, to obtain quantitative spectra. For ^{13}C, 5 ms cross-polarization time with 1 to 10 s recycle time was used. ^1H decoupling time was 20–60 ms in both cases. Chemical shifts were referenced to 85% H_3PO_4 or $(CH_3)_4Si$.

X-Ray photoelectron spectroscopy (XPS). The XPS data were obtained on an automated DuPont 650-photoelectron spectrometer using Mg$K\alpha$ excitation (1254 eV) generated at 300 W. The powdered samples were packed into a cup sample holder, thus eliminating the need of double-faced adhesive tape, normally used for mounting powdered samples. This procedure greatly reduced the amount of carbon contamination on the sample surfaces and thus improved the accuracy of our data by reducing overlayer effects. The data were collected using standard procedures and surface compositions were calculated from the areas of the pertinent photoelectron peaks, using Scofield cross-sections (*18*). The binding energies (E_B) of the photoelectrons were corrected for sample charging effects.

For the majority of the zeolites studied here, the Si_{2p} and Al_{2p} photoelectron peaks were used to calculated Si/Al atomic ratios. The Si_{2s} and Al_{2s} are also available for use but in zeolites having high Si/Al atomic ratios the Al_{2s} peak occurs in the same energy region as the broad energy loss peak from the Si_{2p} photoelectrons. Since it is difficult to evaluate the contribution of the Al_{2s} peak to the composite Al_{2s}–energy loss peak, we are forced to use the Al_{2p} peak in the evaluation of the surface concentration of aluminum.

A special situation arises with zeolites containing cesium and high Si/Al atomic ratios. A cesium photoelectron peak (Cs_{4d}) overlaps with the Al_{2p} and the high Si/Al ratio makes the area measurement of Al_{2s} peak unreliable. To overcome this problem, the cesium contribution is subtracted from the composite Cs_{4d}–Al_{2p} peak to yield the area of the Al_{2p} peak. The area of the Cs_{4d} peak is obtained from a measure of the $Cs_{3d5/2}$ peak and the use of appropriate Scofield cross sections (*18*).

Chemical analyses. Duplicate analyses were obtained on samples equilibrated over saturated ammonium chloride overnight using atomic absorption or atomic emission (ICP) spectrometry.

Sorption characterization. Sorption experiments were performed as described earlier (*3b*).

RESULTS AND DISCUSSION

Methylamines synthesis. The methylamines synthesis, an acid-catalyzed reaction of methanol (MeOH) and ammonia, can be described by the reaction mechanism shown:

$$NH_3 + MeOH \xrightarrow{k_1} MMA + H_2O \quad (1)$$

$$MMA + MeOH \xrightarrow{k_2} DMA + H_2O \quad (2)$$

$$DMA + MeOH \xrightarrow{k_3} TMA + H_2O \quad (3)$$

At the initial stage of the reaction, MMA is the dominant product. As the reaction proceeds, MMA converts to DMA which in turn converts to TMA. Each of these reactions can be described by a rate constant k_1, k_2, and k_3, respectively. If allowed to proceed to completion, this thermodynamically driven reaction will provide an equilibrium product distribution of 15% MMA, 23% DMA, and 62% TMA (mol%). For this case, the ratio of the rate constants k_2/k_3 is about 0.33 at 325°C. If, however, the conversion of DMA to TMA can be sterically inhibited, then the product stream will be richer in DMA. To provide a gauge of our ability to inhibit this conversion, we report the ratio of the rate constants, k_2/k_3, or "selectivity number."

As shown in Table 2, in our examination of various pore-size zeolites, we have found that some untreated zeolites, (*2*) particularly chabazite, (*3*) H-*R*HO, (*4*) and H-ZK-5, (*5*) are effective at producing high dimethylamine selectivities. Because of its unique combination of stability, selectivity, and activity for this reaction, we focused our studies on H-*R*HO.

TABLE 2

Comparison of Selectivity and Activity

Zeolite type	Pore opening[a]	Selectivity number[b]	Activity number[b]
SiO_2/Al_2O_3	—	0.31	0.2
H-Y	12	0.45	0.2
H-Mordenite	12	0.7	1.7
H-Clinoptilolite	10	0.53	0.01
H-Ferrierite	10	0.55	0.02
H-Erionite	8	0.8	0.2
H-Chabazite	8	2.8	0.3
H-*RHO*	8	4.2	3.3
H-ZK-5	8	4.4	0.6

[a] Number of TO_2 groups forming largest ring.

[b] Selectivity number (the ratio of the rate constants k_2/k_3) and activity number (space velocity) under identical reactor conditions (90% methanol conversion, 325°C, 1:1 NH_3 to methanol feed comparison, and 1 atm pressure).

H-*R*HO as prepared by literature procedures yields crystallites on the order of 0.3 to 0.8 μm in size. Typically, impurity phases such as chabazite, pollucite, and zeolite P are also formed (*4, 13, 19*). If the synthesis conditions are well-controlled, the presence of these impurity phases can be limited to approximately 5–10%. The small *R*HO crystallites have an external surface area of approximately 5 to 15 m^2/g based upon their particle size. For a typical preparation of H-*R*HO, the total external surface area, a combination of the accessible surfaces of the impurity and *R*HO phases, can amount to a significant value, 20 to 70 m^2/g, as measured by mercury porosimetry or adsorption (*3b*). The differing amounts of external surface area and impurity phases caused the various *R*HO samples to have a range of selectivities toward the synthesis of DMA versus TMA. Unlike our studies of various sources of chabazite as a methylamines catalyst which showed sorption measurements to provide a rational basis for the catalytic selectivities (*3b*), no such basis could be established for the various zeolite *R*HO preparations. We therefore elected to use their catalytic selectivities, k_2/k_3, as a characterization method.

TABLE 3A

Treatments Applied to a "Substandard" H-*RHO*

Treatment type	Selectivity number[a]	Activity number[a]
Control (nonzeolitic)	0.3	0.2
None (control)	1.9	3.8
TEB	2.3	2.7
HMDS	2.7	3.3
$TiOCl_2$	2.8	2.5
$CiCl_4$	3.6	3.3
Me_3SiCl	4.3	3.3
Me_2SiCl_2	5.6	2.9
PCl_3	7.5	2.6
TMP (sample I)	12.4	2.9

[a] Selectivity number (the ratio of the rate constants k_2/k_3) and activity number (space velocity) under identical reactor conditions (90% methanol conversion, 325°C, 1 : 1 NH_3 to methanol feed composition, and 1 atm pressure).

At room temperature, TMA can neither adsorb nor desorb from the *RHO* framework, but, at temperatures greater than 200°C, it can readily migrate into and out of the framework. Since the methylamines synthesis reaction is performed at 300–325°C over zeolite *RHO*, we expect the TMA formed within the *RHO* framework to be able to enter the product stream. Our efforts to further improve DMA selectivities of *RHO* preparations have involved numerous treatments (*4, 6, 7*) to not only minimize the contribution of the external accessible surfaces but also to narrow the pore openings to prevent TMA from leaving the framework and entering the product stream. These efforts included liquid-phase treatments in which alkoxides were hydrolyzed to give oxide coatings on the zeolite crystallites (*6, 7*). But the most effective treatment involved the vapor-phase reaction of species with the active surface sites.

Selectivity of Vapor-Phase-Treated H-RHO

Some loss in activity is expected by surface treatments as the external surface contributions to the product stream are reduced. However, the contribution to the product distribution by the external surface is expected to be thermodynamically controlled and nonselective and, therefore, the product stream should be richer in TMA. As noted in our earlier work, untreated H-*RHO* is surprisingly selective to DMA versus TMA (*2, 4*). However, the selectivity and activity observed are very dependent upon the nature and amount of impurity phases present as well as the degree of exchange, calcination temperature, and the atmosphere of calcination (*4*). The effect of different vapor-phase treatments on the selectivity and activity of a "substandard" (k_2/k_3 = 1.9) H-*RHO* preparation is shown in Table 3A. The data for a typical nonzeolitic catalyst is provided as a basis of comparison. Indeed, upon application of a surface treatment to a substandard H-*RHO*, modest losses in activity are observed coupled with very significant improvements in selectivity. Clearly, TMP treatment is most effective at improving selectivity. Depending upon the specific preparations of *RHO*, the treatments are so effective that essentially no TMA is observed in the product stream (see Table 3B).

TABLE 3B

Effect of TMP Treatments Applied to Various Samples of H-*RHO*

Sample		Selectivity number[a]	Activity number[a]
Number	Form		
I	Untreated	1.9	3.8
	Treated	12.4	2.9
VI	Untreated	3.3	0.4
	Treated	18.7	0.3
VII	Untreated	3.4	4.3
	Treated	202	3.8
VIII	Untreated	4.5	1.8
	Treated	5700	1.0

[a] Selectivity number (the ratio of the rate constants k_2/k_3) and activity number (space velocity) under identical reactor conditions (90% methanol conversion, 325°C, 1 : 1 NH_3 to mthanol feed composition, and 1 atm pressure).

SCHEME 1

Estimate of Surface and Framework Contributions to the Observed Product Distribution

	Measured product distributions[a]			k_2/k_3
	MMA	DMA	TMA	
Equilibrium[b]	15	23	62	0.33
H-*RHO* (untreated)	16	54	30	3.4
H-*RHO*/TMP	14	86	0.4	202

[a] Basis: 100 moles of product at 90% methanol conversion

[b] Over non-selective catalyst

Step 1. The observed product distribution for the untreated *RHO* sample is MMA = 16, DMA = 54, TMA = 30.

Step 2. Assume that all TMA is produced by the unselective thermodynamically driven reaction at the surface, yielding products in the ratio MMA = 15, DMA = 23, TMA = 62.

Step 3. Calculate the amounts of surface-produced MMA and DMA expected to be in equilibrium with 30 mol of TMA:

(30/62) TMA = (7.3/15) MMA = (11.1/23) DMA.

Step 4. Subtract the surface contribution of MMA (7.3), DMA (11.1), TMA (30) from the observed product distribution to get an apparent bulk contribution:

MMA = 16 − 7.3 = 8.7 DMA = 54 − 11.1
= 42.9 TMA = 30 − 30 = 0.

On a percent basis

$$\text{MMA} = \frac{8.7}{8.7 + 42.9} \times 100 = 16.8 \quad \text{DMA} = 83.1.$$

This calculation indicates the external surface reaction produces an equilibrium product distribution and for this particular sample about one-half of the product stream is coming from the external surface.

Assuming that the external surface of a sample produces TMA with an equilibrium distribution, the contribution of this surface to the product distribution may be estimated, as shown in Scheme 1. The MMA, DMA, and TMA percentages represent distribution on a methanol basis if 100 mol of methanol were converted to methylamines. The external surface contribution is then represented by the ratio of the observed TMA percentage for the untreated catalyst over the equilibrium TMA percentage (62%). Thus, the external surface (before treatment) of a sample provides about 48% (30/62) of the products.

For the *RHO* sample discussed in Scheme 1, the phosphite treatment virtually eliminates the appearance of TMA in the product stream. However, the ability of the phosphite treatment to inhibit TMA production may result not only from deactivation of surface sites, but also from a slight reduction in the channel or pore opening to the surface which may be sufficient to inhibit TMA egress from the framework. To determine the reasons for the improved selectivity, characterization studies involving infrared, MAS-NMR, sorption, XPS and chemical analysis were performed.

Characterization of Surface-Treated H-RHO

Infrared studies. Infrared studies were carried out on samples of H-*RHO* before and after treatment. Relative changes in surface acidity were determined by measuring chemisorbed pyridine at 150°C. Since pyridine is too large to enter the channels of zeolite *RHO*, it chemisorbs at the external (accessible) sites. Separate infrared peaks are observed for the pyridine sorbed on Lewis (approx 1450 cm^{-1}) and Brønsted (approx 1545 cm^{-1}) acid sites. These results are given in Table 4. All vapor-phase treatments decrease the surface acidity and, therefore, reduce the contribution by the surface to the acid-catalyzed methylamines synthesis reaction. Treatment with TMP and PCl_3 stand out as very significantly reducing Lewis acidity in addition to almost eliminating Brønsted acidity. The other treatments, although effective poisons of the Brønsted acidity, are less reactive with the Lewis acid sites. A band at 3740 cm^{-1}, assigned to terminal Si-OH, also significantly decreases in intensity on treatment with HMDS. It is known that these sites in silicas are very reactive with HMDS (*20, 21*). Changes in intensities of internal frame-

TABLE 4

Relative Brønsted and Lewis Acid Site Populations after Treatment

Treatment	Brønsted[a]	Lewis[b]
None	0.020	0.109
HMDS	0.005	0.087
TEB	0.002	0.077
$TiOCl_2$	0.003	0.064
$SiCl_4$	0.003	0.049
Me_3SiCl	0.004	0.036
TMP (sample I)	0.001	0.033
PCl_3	0.002	0.013

[a] IR absorbance of 1545-cm^{-1} peak after pyridine sorption.

[b] IR absorbance of 1450-cm^{-1} peak after pyridine sorption.

work (3640, 3610 cm^{-1}) (*4a*) hydroxyls on treatment are minimal, which suggests that the terminal Si-OH groups are located primarily on the external surface because they are accessible to the vapor-phase treatment by the named compounds. The data indicate that the phosphorus-containing reagents are most effective in decreasing surface acidity.

In the 2850 to 3000-cm^{-1} region, alkyl CH stretches are observed in the infrared spectra of samples treated with TMP and HMDS. These features are very likely due to P-CH_3-, P-OCH_3-, *Z*-CH_3 (*Z* indicates zeolite)-, and/or *Z*-OCH_3-type species. Higher temperatures are apparently needed for more complete dealkylation of the species resulting from the TMP and HMDS treatments.

MAS-NMR studies. As given in Fig. 1A, ^{31}P NMR of a sample of TMP-treated H-*R*HO shows two species:

- one at approximately 35 ppm (with no spinning side bands and no change with/without proton decoupling) and
- one at approximately 2 ppm, *J*(H-P) = 670 Hz of lower intensity, which is assigned to a protonated species.

The protonated species is not present for all TMP-treated H-*R*HO samples. When it is not present as shown in Fig. 1B for the high cesium-containing sample I, ^{31}P NMR shows two overlapping peaks of roughly equal intensity; one at 33.5 ppm (2 ppm width) and one at 35 ppm (9 ppm width) of lower symmetry. The more broadened peak may be the result of an interaction of the absorbed species with the cesium nuclear magnetic moment ($I = 7/2$).

The peak at about 35 ppm in the ^{31}P NMR is significantly different than that of the starting TMP at +140 ppm. This peak is assigned to dimethylmethylphosphonate (DMMP) which is formed by a rearrangement reaction on sorption on the acid zeolite that is similar to the Arbusov (*22*) rearrangement of trialkylphosphites which is shown in Scheme 2. Adsorption of DMMP on large pore HY gave a material very similar to the TMP-treated zeolite that exhibited a peak at +37 ppm in the ^{31}P NMR and peaks at 8, 55, and 53 ppm in the ^{13}C NMR (*23*).

^{13}C NMR of sample II (see Fig. 2A) shows three peaks of roughly equal intensity at 59.4 and 52.3 assigned to P-OCH_3, and at 50.0 ppm assigned to sorbed methanol. Another feature is observed at 7.3 ppm and is assigned to -CH_3. This feature and the one at 59.4 ppm are not observed

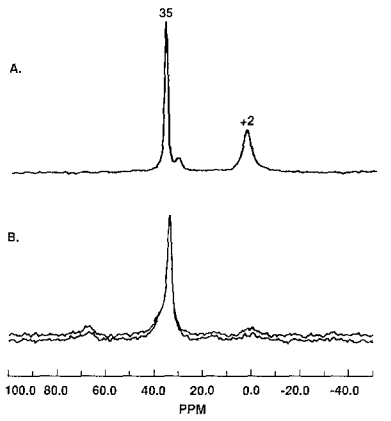

FIG. 1. Room temperature ^{31}P MAS-NMR of (A) sample II (^1H-decoupled) and (B) sample I (superimposition of ^1H-coupled and ^1H-decoupled).

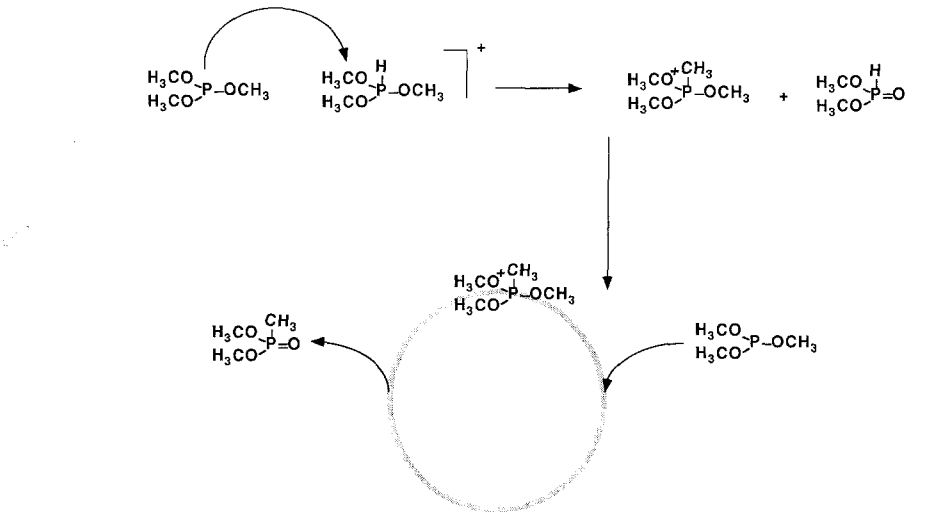

SCHEME 2. Acid-Catalyzed Reaction Sequence Proposed for the Intrazeolite Formation of Dimethyl-methylphosphonate from Trimethylphosphite

for the ^{13}C spectrum of sample I (see Fig. 2B).

In contrast to the small pore zeolites, the large pore zeolite H-Y allows the TMP to access the internal hydroxyl sites. Samples at higher levels of TMP treatment can be prepared and NMR analysis is easier. The ^{31}P NMR of a TMP-treated sample of H-Y, given in Fig. 3A, shows two peaks—one at 36 and one at 22 ppm. As noted above, the peak at 36 ppm is assigned to DMMP. The ^{13}C NMR, given in Fig. 4A, shows two inequivalent methoxy groups at 55 and 53 ppm and a smaller peak at 8.5 ppm assigned to P-CH_3. The two methoxy peaks (which are also observed with H-*R*HO) are tentatively assigned to free and protonated DMMP, respectively. IR studies (*23*) showed proton transfer from both supercage and weaker acid sites toward the adsorbed phosphorus compound as observed in the hydroxyl region and indicated by a broad 2440-cm^{-1}

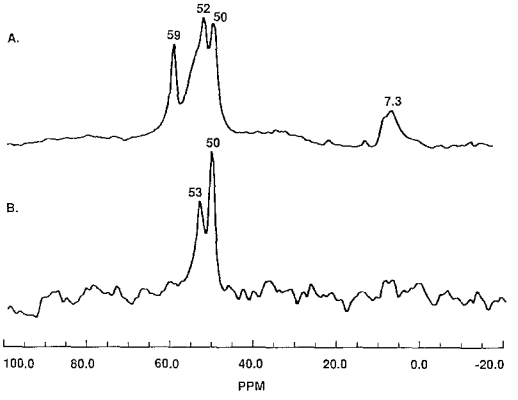

FIG. 2. ^{13}C MAS-NMR at room temperature for (A) sample II and (B) sample I.

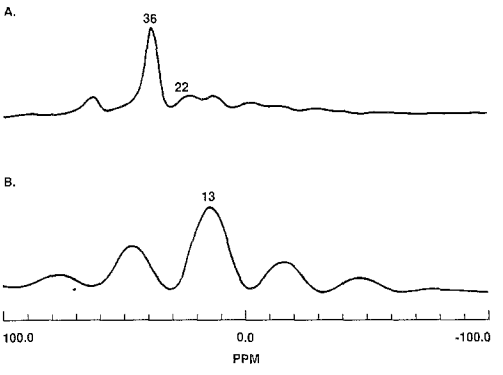

FIG. 3. ^{1}H-Decoupled ^{31}P MAS-NMR of H-Y (A) saturated with TMP at room temperature and (B) degassed at 400°C for 12 h.

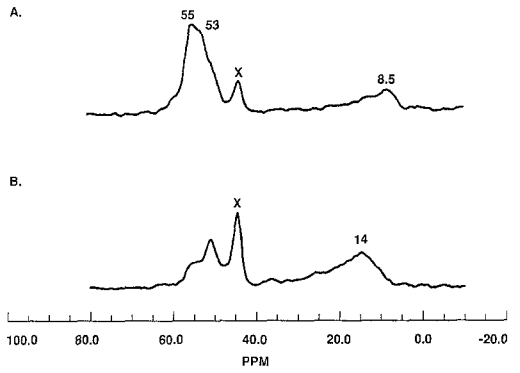

FIG. 4. Cross-polarized and ^{1}H-decoupled ^{13}C MAS-NMR of H-Y (A) saturated with TMP at room temperature and (B) degassed at 400°C for 12 h.

band (see Fig. 5A). Evidence for the nature of the reaction product is found in the C-H bending region. The new methyl group is represented by a band at 1305 cm^{-1}, whereas a pair at 1460/30 cm^{-1} accounts for the methoxy group. In addition, a shoulder at 1250 cm^{-1} is probably due to the newly generated P=O double bond.

Heating the phosphite-loaded wafer in the IR cell under vacuum (1 h at 160 and at 340°C) reduces the overall C-H intensity, as shown in Figs. 5B and 5C). However, the hydroxyl bands are not restored as would be expected upon simple dissociation of a phosphonium species. In contrast, the OH- intensity decreases with heating time, indicating an irreversible reaction with the phosphorus compound. NMR data provide further evidence for the species obtained upon thermal desorption treatments. On degassing at 400°C for 12 h, the rearrangement product DMMP transforms to another species with a ^{31}P resonance at +13 ppm and a strong anisotropy as indicated by the sideband intensity in Fig. 3B. This species is tentatively assigned to a zeolite-bound (=$P(O)CH_3$) fragment. The ^{13}C spectrum of TMP heated in H-Y at 300°C for 12 h given in Fig. 4B substantiates the findings of the IR experiments, i.e., the methoxy bands are considerably smaller compared to the room temperature system. Also, a large fraction of methyl groups is indicated by the resonance at 14 ppm. Both the IR and NMR results suggest that the rearrangement product DMMP reacts irreversibly with the zeolite hydroxyl groups upon heating under vacuum. This reaction is accompanied by a loss of methoxy groups which probably desorb from zeolite H-Y as methanol. Similar behavior has been reported by Weinberg and coworkers for the reaction of DMMP adsorbed onto Al_2O_3 (*24*). In the small pore *RHO* system, the methanol, thus formed, could be readily readsorbed (as indicated by the ^{13}C NMR feature at 50.0 ppm).

XPS. XPS measurements were obtained to determine the relative surface composition and nature of the surface species of the TMP-treated samples. The binding energy (E_B = 134.0 ± 0.2 eV) of the P_{2p} photoelectron peak for all samples indicates pentavalent phosphorus bonded to oxygen. The atomic ratio values from chemical analysis and XPS are given in Table 5 for a series of TMP-treated H-*RHO* samples that were heated after the vapor-phase treatment. The surface/bulk ratio for phosphorus analysis is greater than one for all samples, indicating surface enrichment of this element. Similar data for other zeolites treated with TMP are summarized in Table 6. The most striking result is the homogeneous distribution of P in H-Y zeolite, indicating that the internal structure of this zeolite is accessible to TMP.

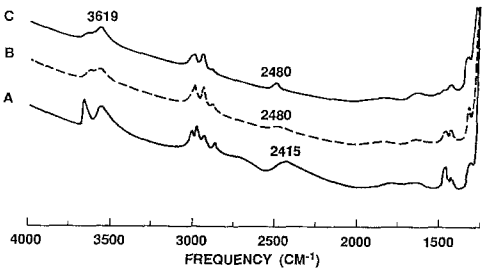

FIG. 5. IR spectra of a wafer of H-Y, degassed at 400°C, loaded with TMP at room temperature (5.5 Torr) and degassed (A) at room temperature for 30 min, (B) at 170°C for 60 min, and (C) at 340°C for 60 min.

TABLE 5

XPS of TMP-Treated *RHO* Zeolites

Sample	Si/Al ratio			(D) (Si + Al)/O	P Analysis		
	(A) Bulk[a]	(B) Surface[b]	(C) Surface/ bulk		(E) Bulk[a] P/(Si + Al)	(F) Surface[b] P/(Si + Al)	(G) Surface/ bulk
I	2.8	1.3	0.46	—	0.012	0.051	4.2
II	3.3	5.6	1.68	0.28	0.030	0.36	12.0
III	3.3	6.2	1.89	0.24	0.035	0.49	14.0
IV	3.3	4.3	1.32	0.31	0.027	0.28	10.4
V	3.7	4.2	1.12	0.30	0.060	0.22	3.7

[a] Chemical analysis (±2–5%).
[b] XPS analysis.

Sorption measurements. Sorption data, given in Table 7, obtained before and after treatment of the *RHO* samples, indicate that virtually no change in capacity has occurred; therefore, the framework has not been affected by treatment. (This is supported by the fact that essentially no change in the X-ray powder diffraction patterns before and after treatment was observed.) Measurements of relative sorption rates comparison of *n*-propanol uptake (at 20 and 136 h) are very sensitive to small changes in the dimensions of pore openings and these also did not change significantly upon treatment. Therefore, the sorption measurements indicate that only the external surface

TABLE 6

XPS of TMP-Treated Zeolites

Zeolite	Si/Al ratio			(D) (Si + Al)/O	P Analysis			(H) Largest pore[c]
	(A) Bulk[a]	(B) Surface[b]	(C) Surface/ bulk		(E) Bulk[a] P/(Si + Al)	(F) Surface[b] P/(Si + Al)	(G) Surface/ bulk	
H-Y	2.9	1.2	0.43	0.45	0.27	0.267	0.99	12
H-ZSM-34	5.0	4.8	0.96	0.54	0.040	0.045	1.1	12
H-ZK-5	3.0	1.8	0.60	0.67	0.034	0.057	1.7	8
H-*RHO* (sample I)	2.8	1.3	0.46	—	0.012	0.051	4.2	8
H-Erionite	3.5	3.5	1.00	0.46	0.008	0.056	6.9	8
H-Offretite	3.5	3.2	0.91	0.50	0.006	0.045	8.2	12
H-Clinoptilolite	4.9	2.2	0.50	0.57	0.003	0.034	11.3	10
H-T	3.7	1.7	0.47	0.44	0.030	0.415	14.0	12
H-Chabazite	3.8	3.2	0.84	0.50	0.004	0.072	16.4	8
H-Ferrierite	4.6	3.6	0.78	0.46	0.002	0.068	40.0	10

[a] Chemical analysis (±2–5%).
[b] XPS analysis.
[c] Number of TO_2 units in largest pore opening.

TABLE 7

Sorption Results[a] on Vapor-Phase-Treated H-*RHO*

Treatment type	Surface area (m^2/g)	Methanol (20 h)[b]	*n*-Propanol (20 h)[c]	*n*-Propanol (136 h)
None	55.9	13.68	1.72	7.7
TMP (sample I)	39.7	13.35	8.22	11.8
Me_2SiCl_2	70.3	14.74	3.86	13.7
Me_3SiCl	40.1	14.26	5.95	12.5
$SiCl_4$	41.6	14.16	4.98	12.2
HMDS	41.2	13.72	2.05	11.1
$TiOCl_2$	54.0	12.97	1.85	6.8
TEB	59.6	13.93	5.83	12.0

[a] Grams of solvent (methanol, *n*-propanol) absorbed per 100 g dry sample at 20–25°C.

[b] Equilibrium value which provides a measure of the sorption capacity for a given sample.

[c] With no sorption constraints, this would equal the methanol value since both species have the same density.

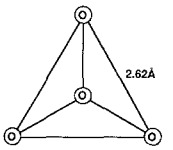

Area (1 Side of TO_2 Tetrahedron) = $\frac{1}{2}$ b x h = $\frac{1}{2}$(2.62)(2.62)sin 60° = 2.97Å^2

Area (4 Sides of TO_2 Tetrahedron) = 11.89Å^2

$$\text{Surface Area} = \frac{(11.89\ \text{Å}^2/\ TO_2)\ (6.023 \times 10^{23}\ TO_2/\ \text{mole})}{(10^{20}\text{Å}^2/\ \text{m}^2)\ (60.0\ \text{g}/\ \text{mole})} = 1200\ \text{m}^2/\ \text{g}$$

SCHEME 3. Surface Area Calculation for TO_2 Tetrahedron

(and not the framework) of the *RHO* zeolite is modified by these vapor-phase treatments.

Titration of external sites as a measure of external surface area. For small pore zeolites, as noted above, the vapor-phase treatments seem to titrate only the external surface of the zeolite particles. A comparison can then be made between the surface areas obtained from mercury porosimetry, adsorption of large molecules, and the vapor-phase titrations. The XPS data in Table 6 indicate that, for small pore zeolites, the majority of the phosphorus is found in the surface layers, as expected. Assuming that the surface acid sites are titrated in the vapor-phase treatment, then chemical analysis should provide a measure of the external surface area. Using a TO_2 tetrahedron as the basic building unit with all four sides available for adsorption and an O–O bond distance of 2.62 Å, as in quartz, yields a calculated surface area of approximately 1200 m^2/g as shown in Scheme 3. Substituting some Al for Si does not appreciably change this value.

Using the assumptions:

(1) a uniform aluminum distribution throughout the zeolite,

(2) a total surface area of about 1200 m^2/g,

(3) the kinetic diameter of the TMP molecule (and the DMMP product) is too large to enter the zeolite pores at the treatment temperatures,

(4) TMP reacts with a site associated with the surface aluminum, and

(5) negligible physisorption occurs,

then, the percentage Al and percentage P obtained from chemical analysis provide a measure of the "treated" surface area. A typical calculation is given in Scheme 4 and

TABLE 8

Selective Titration of External Acid Sites as a Measure of External Surface Area

Zeolite type	"Treated" (m^2/g)	Experimental[a] (m^2/g)	Largest pore[b]
H-chabazite	24.4	11.5, 25[c]	8
H-ZK-5	40.9	37.4	8
H-erionite	43.4	38.3	8
H-RHO (sample I)	61.0	55.9	8
H-ferrierite	11.2	10.3	10
H-clinoptilolite	22.0	34.9	10
H-offretite	111.9	40.	12
H-T	169.	—	12
H-ZSM-34	287.	—	12
H-Y	1260	—	12

[a] Hg porosimetry/sorption external surface area for untreated sample.

[b] Number of TO_2 groups forming largest ring.

[c] 11.5 m^2/g from Hg porosimetry; 25 m^2/g from sorption.

H-Ferrierite

5.94% Al
0.064% P

$$\frac{(0.0594\ \text{g}/26.982\ \text{g/mole})}{1200\ \text{m}^2/\text{g}} \times \frac{6.023 \times 10^{23}\ \text{Al/mol}}{10^{20}\ \text{Å}^2/\text{m}^2} = 1.1\ \text{Al}/100\ \text{Å}^2$$

$$\frac{(0.00064\ \text{g}/30.974\ \text{g/mol})}{x\ \text{m}^2/\text{g}} \times \frac{6.023 \times 10^{23}\ \text{Al/mol}}{10^{20}\ \text{Å}^2/\text{m}^2} = 1.1\ \text{Al}/100\ \text{Å}^2$$

$$x \cong 11.1\ \text{m}^2/\text{g}$$

SCHEME 4. Example Calculation

the results for a variety of zeolites are given in Table 8. For comparison, external surface areas obtained from combined mercury porosimetry and sorption data are also given.

For both the small pore (8-ring) and medium pore (10-ring) zeolites, there is very good agreement between the treated areas and those obtained from porosimetry and/or adsorption. The treated surface areas of the large pore (12-ring) zeolites are much larger than those of the small pore zeolites as expected, because TMP enters the large channels and reacts with internal acid sites. In the case of H-Y, the TMP has reacted with all of the acid sites as indicated by the treated area equalling the total available area. In the offretite-containing zeolites (H-T, H-ZSM-34, and H-offretite), the 12-ring channels are one-dimensional and do not open into large cages as in H-Y. Hence, once the TMP reacts with an acid site in the channel it will effectively block other TMP molecules from entering and reacting within that channel.

CONCLUSIONS

The results presented here show that vapor-phase treatment of zeolite H-*R*HO is very effective in improving the selectivity to dimethylamine in synthesis from methanol and ammonia by eliminating the nonselective surface reactions which produce predominantly TMA. Infrared characterization studies have shown that phosphorous-containing vapor-phase treatments are especially effective at reducing or eliminating surface acidity as measured by pyridine chemisorption. Reaction of these Brønsted and Lewis acid sites deactivates the external (nonselective) catalytic sites. MAS-NMR studies have shown that TMP reacts irreversibly with the zeolite acidic sites via a modified Arbusov rearrangement to form surface bound DMMP. Since no significant change in sorption capacity and sorption rate occurs upon vapor-phase treatment with TMP, we can exclude pore-size narrowing as a significant factor for the improved catalytic selectivity of the zeolite.

ACKNOWLEDGMENTS

The authors acknowledge the contribution of R. H. Staley, who carried out some of the infrared experiments, as well as the technical assistance of R. W. Shiffer, C. E. Perry, E. T. Jones, Jr., W. B. Arters, E. M. Riley, and R. F. Carver.

REFERENCES

1. Weigert, F. J., *J. Catal.* **103,** 20 (1987).
2. Keane, M., Sonnichsen, G. C., Abrams, L., Corbin, D. R. Gier, T. E., and R. D. Shannon, *Appl. Catal.* **32,** 361 (1987).
3. (*a*) Abrams, L., Shannon, R. D., and Sonnichsen, G. C., US Patent 4,737,592, 1988; (*b*) Abrams, L., Keane, M., Jr., and Sonnichsen, G. C., *J. Catal.* **115,** 410 (1989).
4. (*a*) Shannon, R. D., Keane, M., Jr., Abrams, L., Staley, R. H., Gier, T. E., Corbin, D. R., and Sonnichsen, G. C., *J. Catal.* **113,** 367 (1988); (*b*) Shannon, R. D., Keane, M., Jr., Abrams, L., Staley, R. H., Gier, T. E., Corbin, D. R., and Sonnichsen, G. C., *J. Catal.* **114,** 8 (1988); (*c*) Gier, T. E., Shannon, R. D., Sonnichsen, G. C., Corbin, D. R.,

and Keane, M., Jr., US Patent 4,806,689, 1989; (*d*) Abrams, L., Corbin, D. R., and Shannon, R. D., US Patent 4,814,503, 1989.
5. Gier, T. E., Shannon, R. D., and Sonnichsen, G. C., US Patent 4,602,112, 1986; Shannon, R. D., Keane, M., Jr., Abrams, L., Staley, R. H., Gier, T. E., and Sonnichsen, G. C., *J. Catal.* **115,** 79 (1989).
6. Bergna, H. E., Corbin, D. R., and Sonnichsen, G. C., US Patent 4,683,334, 1987; Bergna, H. E., Corbin, D. R., and Sonnichsen, G. C., US Patent 4,752,596, 1988.
7. Bergna, H. E., Keane, M., Jr., Ralston, D. H., Sonnichsen, G. C., Abrams, L., and Shannon, R. D., *J. Catal.* **115,** 148 (1989).
8. *TIME*, October 4, 1982.
9. Treatment with phosphorus, boron, aluminum [Lindsley, US Patent 3,753,929; Nozemack, US Patent Application 2,079,737], silicon [Yang, US Patent 4,452,909].
10. Dejaifve, P., Auroux, A., Gravelle, P. C., Vedrine, J. C., Gabelica, Z., and Derouane, E. G., *J. Catal.* **70,** 123 (1981).
11. Corbin, D. R., Seidel, W. C., Abrams, L., Herron, N., Stucky, G. D., and Tolman, C. A., *Inorg. Chem.* **24,** 1800 (1985).
12. Corbin, D. R., Abrams, L., and Bonifaz, C., *J. Catal.* **115,** 420 (1989); Corbin, D. R., Bonifaz, C., and Abrams. L., *in* "Catalysis 1987" (J. W. Ward, Ed.), pp. 295–302. Elsevier, Amsterdam, 1988.
13. Robson, H. E., US Patent 3,904,738, 1975.
14. Robson, H. E., US Patent 3,720,753, 1973.
15. Rollman, L. S., and Volyoscik, E. W., *Inorg. Synth.* **22,** 61 (1983).
16. Breck, D. W. and Acara, N. A., US Patent 2,950,952, 1960.
17. Ruben, M. K., Rosinski, E. J., and Plank, C. J., US Patent 4,086,186, 1978.
18. Scofield, J. H., *J. Electron Spectrosc.* **8,** 129 (1976).
19. Barrer, R. M., Barri, S., and Klinowski, J., *in* "Proceedings, 5th International Zeolite Conference" (L. V. Rees, Ed.), pp. 20–29. Heyden, London, 1980.
20. Hertl W. and Hair, M. L., *J. Phys. Chem.* **75,** 2181 (1971).
21. Bein, Th., Carver, R. F., Farlee, R. D., and Stucky, G. D., *J. Amer. Chem. Soc.* **110,** 4546 (1988).
22. Arbuzov, A. E., *Russ. J. Phys. Chem. Soc.* **46,** 291 (1914).
23. Bein, Th., Chase, D. B., Farlee, R. D., and Stucky, G. D., *in* "New Developments in Zeolite Science Technology" (Y. Murakami, A. Iijima, and J. W. Ward, Eds.), pp. 311–318. Kodansha, Tokyo, 1986.
24. Templeton, M. K., and Weinberg, W. H., *J. Amer. Chem. Soc.* **107,** 97 (1985); Templeton, M. K. and Weinberg, W. H., *J. Amer. Chem. Soc.* **107,** 774 (1985).